CRYSTAL GROWTH & DESIGN

pubs.acs.org/crystal

Article

Balancing Color and Hardness in $ZnO-Al_2O_3-SiO_2$ Glass-Ceramics by Tailoring the ZrO_2/TiO_2 Nucleating Agents Ratio

Lorena Raphael Rodrigues,* Gisele Guimarães dos Santos, María Helena Ramírez Acosta, Akio Koike, Shusaku Akiba, Shigeki Sawamura, Satoshi Yoshida, Valmor Roberto Mastelaro, Otaciro Rangel Nascimento, and Edgar Dutra Zanotto

Cite This: *Cryst. Growth Des.* 2024, 24, 9914−9924

Read Online

ACCESS | Metrics & More | Article Recommendations | Supporting Information

ABSTRACT: Transparent and hard $ZnO-Al_2O_3-SiO_2$ (ZAS) glass-ceramics (GCs) are desirable for various applications. However, TiO_2, an effective nucleating agent for this system, can introduce an unwanted yellow coloration. This study explores the effect of partially replacing TiO_2 with ZrO_2 on the crystallization pathways, color, transparency, and hardness of ZAS glasses and corresponding GCs, by evaluating compositions containing a constant content (4.5 mol %) of the referred nucleating agents. Optical transmittance showed that all glasses and GCs prepared were transparent in the visible range. However, they presented a yellowish hue that faded as the ZrO_2/TiO_2 ratio increased, as indicated by the CIELab analyses. One possible source of such coloration is the presence of iron ions in different oxidation states such as Fe^{2+} and Fe^{3+}, this last detected by Electron Paramagnetic Resonance measurements in all the glasses. The samples' color is also likely affected by the $Ti^{4+}-O^{2-}$ charge transfer mechanism. Concerning the mechanical performance, all GCs present similar hardness, which is a consequence of the slight variation in the crystallization kinetics with the varying ZrO_2/TiO_2 ratio. Therefore, the partial replacement of TiO_2 with ZrO_2 enables the preparation of glasses and GCs with a lighter coloration, without impairing their hardness.

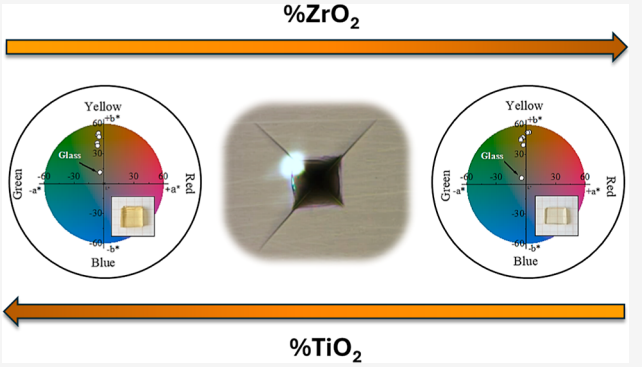

1. INTRODUCTION

Glass-ceramics (GCs) are inorganic, polyphasic materials obtained through the controlled crystallization of some inorganic, nonmetallic glasses.[1] This thermally activated process involves crystal nucleation and growth of at least one functional crystalline phase in the bulk or surface region of the parent glass. Although the crystal fraction can vary from ppm to almost 100 vol %,[1] most commercially available GCs typically exhibit a crystallized fraction of less than 70%. The final nano- or microstructure is a consequence of the chemical composition of the parent glass and subsequent heat treatment protocols. The unlimited and precise combination of all these factors has enabled the tuning of GCs' properties to achieve the most demanding technological requirements in diverse fields, including medicine,[2] dental,[3] ballistic,[4] optoelectronic,[5] energy,[6,7] and telecommunication,[8] among others.

This study focuses on the production of GCs combining optical transparency and good mechanical performance, which are essential for several applications, such as displays for electronic devices,[9] bulletproof armors,[4] and telescope mirrors.[10,11] However, successfully achieving this combination of properties in GCs is particularly challenging since the improvement of one often comes at the expense of the other. For instance, nanosized crystals are usually required for transparency, while good mechanical properties are mainly associated with a relatively coarse microstructure (μm scale instead of nm) and high crystalline fraction,[12] characteristics that tend to result in optically opaque GCs.

Obtaining transparent GCs requires minimum light scattering; therefore, the material should present crystals much smaller than the wavelength of visible light (nanometric crystals), or, in the case of micrometric crystals, the crystalline and vitreous phases should have similar refractive indexes.[13] Usually, the smaller the crystals and the closer the refractive index of the different phases, the higher the light and image transmittance.

Some glass compositions from which it is possible to produce transparent, harder, and tougher GCs have been discovered in the $ZnO-Al_2O_3-SiO_2$ (ZAS) system.[14]

Received: July 19, 2024
Revised: November 13, 2024
Accepted: November 13, 2024
Published: November 20, 2024

https://doi.org/10.1021/acs.cgd.4c01000
Cryst. Growth Des. 2024, 24, 9914−9924

However, to boost the crystal nucleation in ZAS-based GCs, reaching a crystal number density high enough to yield a transparent material while preserving the mechanical performance, it is necessary to add nucleating agents to the parent glass. These compounds are added in relatively small quantities, usually lower than 7 mol %, and they act by lowering the thermodynamic or kinetic energy barrier, or both, for the crystal nucleation of the parent glass.[15] In ZAS glasses, TiO_2 is commonly used as a nucleating agent,[14,16] however, this compound usually alters the visible light absorption of the silicate glasses and corresponding GCs, giving them a yellowish or brownish hue[14,17,18]—an undesired effect for some applications such as electronic displays and ballistic shielding. It is believed that the main source of this coloring effect in the glass and GCs is the presence of Ti^{3+} cations, which show a $3d^1$ electronic configuration with a d−d absorption band close to 500 nm.[19] An attempt to attenuate or avoid this effect is the addition of clarifying compounds such as CeO_2, which acts as an oxidizing agent for Ti^{3+} ions.[14] Iron ions—a common impurity in glass-making raw materials—can also give coloration to the glass and GCs containing TiO_2, because of selective light absorption by Fe^{3+} and Fe^{2+} ions that can contribute to a charge transfer with Ti^{3+} and Ti^{4+} ions.[17] Due to these divergent hypotheses, there is no definitive conclusion on whether titanium or iron ions are responsible for the yellowish tone of ZAS GCs containing TiO_2 as a nucleating agent.

Another alternative to mitigate the undesirable coloration, apparently induced by TiO_2, is to replace it with another effective nucleating agent, for instance, ZrO_2, also commonly incorporated into several aluminosilicate glass compositions to boost internal nucleation.[20−23] The addition of ZrO_2 usually does not affect the glass and GCs' color, since the absorption associated with the charge transfer of O^{2-}−Zr^{4+} is expected to occur in wavelengths around 165−195 nm,[24] out of the visible range. Motivated by this possibility, in this study, we evaluate the effect on the crystallization and some properties (color, transmittance, and hardness) of GCs from three ZAS compositions with varying ZrO_2/TiO_2 ratios, while maintaining the overall nucleating agent content constant (4.5 mol %). Thus, the main goal of this research is to identify the most effective ZrO_2/TiO_2 ratio for achieving a combination of high transparency, colorless appearance, and high hardness in ZAS glasses and GCs. Also, we are interested in understanding the origin of the yellowish tone of these glasses and GCs.

2. EXPERIMENTAL SECTION

2.1. Glass Preparation. The nominal chemical compositions of the glasses from the ZnO−Al_2O_3−SiO_2 (ZAS) system selected for this study are presented in Table 1. The composition ZAS A was taken from ref 14 whereas ZAS B and ZAS C have the same nominal content of ZnO, Al_2O_3, and SiO_2 of ZAS A but a varying ZrO_2/TiO_2 ratio.

ZnO, Al_2O_3, and SiO_2 (ZAS) are the main constituents for forming cubic gahnite ($ZnO{\cdot}Al_2O_3$) crystals; K_2O is added to decrease the liquid viscosity and aid in the melting of this high-alumina glass. ZrO_2 and TiO_2 act as nucleating agents, while CeO_2 is added to mitigate the yellowish color of the glass. These glass compositions lead to the formation of gahnite as the main crystal phase upon crystallization.

For each composition, 100 g of glass were prepared using the following chemicals: SiO_2 (Zetasil 2, >99.9%), Al_2O_3 (Almatis, 99.0%), ZnO (Synth, 99.0%), TiO_2 (Riedel de Haen, 99.8%), ZrO_2 (Alfa Aesar, 99.5%), K_2CO_3 (Sigma-Aldrich, >99.0%), and CeO_2 (Vetec, 99%). The chemicals were previously dried in an oven at ~100 °C for 24 h, weighted and mixed according to the nominal composition given in Table 1, and then homogenized in a high-speed mixer at 1200 rpm for 5 min. The batch was melted in a Deltech electric furnace at approximately 1600 °C for 3 h, using a Pt crucible. To improve the chemical homogeneity, the melt was poured, crushed, and remelted three times. Glass plates of ~4 mm thickness were obtained through a splat cooling procedure by pouring the melts and pressing them between two flat metallic plates. To relieve internal stress, the glass plates were annealed at 50 °C below the glass transition temperature (T_g) for 2 h, using heating and cooling rates of 3 and 1 °C/min, respectively.

Table 1. Nominal Composition of the ZAS Glasses Analyzed (in Mol %)

components	ZAS A	ZAS B	ZAS C
SiO_2	60.7	60.7	60.7
Al_2O_3	16.2	16.2	16.2
ZnO	16.2	16.2	16.2
K_2O	2.2	2.2	2.2
CeO_2	0.2	0.2	0.2
TiO_2	4.5	2.25	1.5
ZrO_2		2.25	3.0

2.2. Thermal Analysis and Crystallization Kinetics. The characteristic temperatures of the glasses, such as T_g, and the crystallization onset (T_x) and peak (T_p) temperatures were determined by differential scanning calorimetry (DSC). The DSC measurements were performed in a differential scanning calorimeter (model Netzsch 404), using monolithic glass pieces (~30 mg) inserted in a Pt pan and lid set, and a heating rate of 10 °C/min from room temperature to 1200 °C. Additionally, DSC analyses were employed to estimate the temperature of the maximum nucleation rate ($T_{n\text{-}max}$) for each glass, using a nonisothermal method based on the (T_p) shift and the variation in the crystallization peak height (P_H) for different nucleation temperatures (T_n).[25] This qualitative analysis of $T_{n\text{-}max}$ was performed considering the results of T_p indicated by the DSC curves, also obtained from monolithic samples previously submitted to varying nucleation treatments of 2 h at $T_n = T_g$, T_g−10 °C, T_g +10 °C and T_g +20 °C.

The Kissinger model,[26] given by eq 1, was used to estimate how the activation energy (E_a) for the crystallization is affected by the different proportions of nucleating agents. This equation considers the shift of T_p with the temperature when increasing the heating rate (φ) used in the DSC runs. For this analysis, the DSC measurements were conducted using different heating rates (15, 20, 25, and 30 °C/min) in bulk samples of approximately 40 mg. In eq 1, R is the gas constant.

$$\ln\left(\frac{T_p^2}{\varphi}\right) = -\frac{E_a}{RT_p} + \text{constant} \quad (1)$$

2.3. Heat Treatment Protocol and Characterization. Thermal analyses were performed to guide the heat treatment protocols for each glass to produce the GCs. To this end, double-stage heat treatments were implemented, comprising the nucleation of crystals at $T_n = T_{n\text{-}max}$ and their growth at the T_x and T_p temperatures observed in the DSC curves. Table 2 summarizes the implemented heat

Table 2. Heat Treatments Conducted in the ZAS Glasses

nucleation		growth		nomenclature
temperature [°C]	time [h]	temperature [°C]	time [h]	
$T_n = T_{n\text{-}max}$	3	T_x	2	A/B/C-1
		T_p		A/B/C-2
	24	T_x		A/B/C-3
		T_p		A/B/C-4
	48	T_x		A/B/C-5
		T_p		A/B/C-6

https://doi.org/10.1021/acs.cgd.4c01000
Cryst. Growth Des. 2024, 24, 9914−9924

treatments and the identification of each sample. The adopted identification system for the samples is based on the composition name (ZAS A, B, and C) and the heat treatment protocol (crystal nucleation time and crystal growth temperature) used. It is important to note that, for comparison purposes, the same heat treatment conditions, considering the characteristic temperatures of each glass (Table 3), were applied to all compositions.

Table 3. Glass Transition (T_g), Crystallization Onset (T_x), and Peak (T_p) Temperatures of the ZAS Glasses[a]

glass	T_g [°C]	T_x [°C]	T_p [°C]
ZAS A	668	790	835
ZAS B	715	900	923
ZAS C	719	870	884

[a]The estimated error in these temperatures is less than ±3 °C.

To identify the crystalline phases in the GCs, X-ray diffraction (XRD) analyses were conducted in bulk pieces, after removing the surface crystallized layer, using a diffractometer (Rigaku Ultima IV) with a Cu K_α radiation source, a scanning interval (2θ) from 10 to 80°, a step scan of 0.02°, and a counting time of 1 s. The average crystallite size (D) of the GCs was inferred from the XRD diffractograms through the Scherrer equation according to eq 2.

$$D = \frac{K\lambda}{\beta \cos\theta} \tag{2}$$

where K is the Scherrer constant (~0.9 for any crystallite shape[27]); λ is the wavelength of X-ray radiation (Cu Kα = 1.5406 Å); β is the full width at half-maximum of the most intense diffractogram peaks; and θ is the Bragg angle. To avoid biased results, D was estimated considering the five most intense peaks.

Since the XRD instrument itself can contribute to the broadening of the diffraction peaks, a correction was implemented to avoid underestimating D. To this end, a XRD measurement was run on a crystalline SiO_2 (quartz) sample using the same conditions as those applied to the GCs. Since in this case, β should be almost zero, any value associated with this parameter can be attributed to the instrumental contribution to peak broadening. Therefore, for the correction, the found value (β = 0.1334°) was subtracted from those initially estimated for the GCs.

The light transmittance and the color of the parent glasses and GCs were evaluated in a PerkinElmer UV/vis spectrometer, in the wavelength ranges λ = 800−300 nm and λ = 780−380 nm, respectively, with a scan speed of 60 nm/min. For these measurements, samples of approximately 3.0 mm thickness were used. The largest parallel faces were ground with SiC paper of different granulometry (from 320 to 1200 mesh) and polished using a velvet cloth moistened with an aqueous CeO_2 suspension.

The color analysis was performed following the guidelines of the Commission Internationale de ÍEclairage (CIE or CIELab from CIE L*a*b*). The CIELab is a color space system used to measure and describe the perception of colors consisting of 3 coordinates: "a*" (red and green axis, where + a* indicates red and − a* indicates green), "b*" (yellow and blue axis, where + b* indicates yellow and − b* indicates blue), and *L, which varies from black (0) to white (100), indicating the lightness of the color.[28,29] The a* and b* coordinates have no fixed boundaries.[28] In this study, the colorimetric coordinates of each sample were determined in the CIE 1931 system through the PerkinElmer Color software considering a 2° observation angle. Despite some limitations,[30] the CIELab is still one of the most used color spaces.

To verify whether Fe^{3+} or Ti^{3+} could be considered the main source of the coloration of the glasses and GCs, we conducted electron paramagnetic resonance (EPR) measurements in the glasses and some GCs (A6, B6, and C6) from compositions ZAS A, ZAS B, and ZAS C. To collect the EPR spectra, polished samples of ~2 × 2 × 10 mm were inserted into a quartz tube with an internal diameter of 3 mm. Cr^{3+} was used as a standard of g values to calibrate the magnetic field (g = 1.9797). The tests were conducted in a Varian E-109 X-band spectrometer at two temperatures: 295 and 77 K. The following measurement parameters were used: center field = 260 mT, scan range = 500 mT, sweep time = 180 s, number of points = 4096, microwave power = 20 mW, modulation amplitude = 0.2 mT, modulation frequency = 100 kHz, and microwave frequency = 9.10661 GHz.

Vickers microhardness (H_v) was determined for the parent glasses and GCs. This mechanical test was conducted on polished samples (prepared using the same procedure for the transmittance samples) in an Anton Paar MHT device with a square-based diamond pyramid indenter. A load of 10 N was applied for a dwell time of 15 s (at an average temperature of 20 °C and humidity of ~55%). For the calculation of H_v, at least five valid indentations (symmetric indentations with a difference between the two diagonal lengths lower than 5% of the average value, and without excessive cracking around the indentation) were considered for each sample.[31] The H_v [GPa] was calculated via eq 3

$$H_v = 0.001854\frac{P}{d^2} \tag{3}$$

where P is the load [N] and d is the average length [mm] of the diagonals of the impressions.

3. RESULTS

3.1. Thermal Analysis and Crystallization Kinetics.

The DSC curves of each glass composition, as well as their external appearance, are shown in Figure 1. For ease of comparison, the characteristic temperatures T_g, T_x and T_p, are summarized in Table 3.

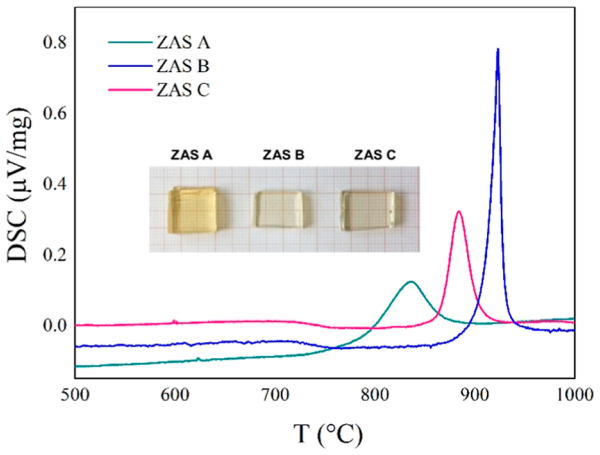

Figure 1. DSC traces of the parent glasses ZAS A, ZAS B, and ZAS C obtained at a heating rate of 10 °C/min. The visual appearance of the glasses is shown in the inset.

Based on the T_g values, four to five different T_n were chosen for the qualitative analysis of $T_{n\text{-}max}$. The relative position of T_p is expected to be proportional to the internal nuclei number density (N_v)[32] since a high number of nuclei contributes to faster crystallization kinetics, which shifts T_p to lower temperatures. Thus, the maximum of the $1/T_p$ ratio should occur for samples heat-treated at a T_n corresponding to the highest nucleation rate. For the cases in which the $1/T_p$ vs T_n trend is not conclusive, i.e., $1/T_p$ keeps increasing with T_n, the behavior of the P_H vs T_n curve should be considered. A decrease in P_H with an increasing T_n indicates an overlap between the nucleation and crystal growth curves, and such overlap also leads to an increase in the $1/T_p$ ratio. Figure 2

https://doi.org/10.1021/acs.cgd.4c01000
Cryst. Growth Des. 2024, 24, 9914−9924

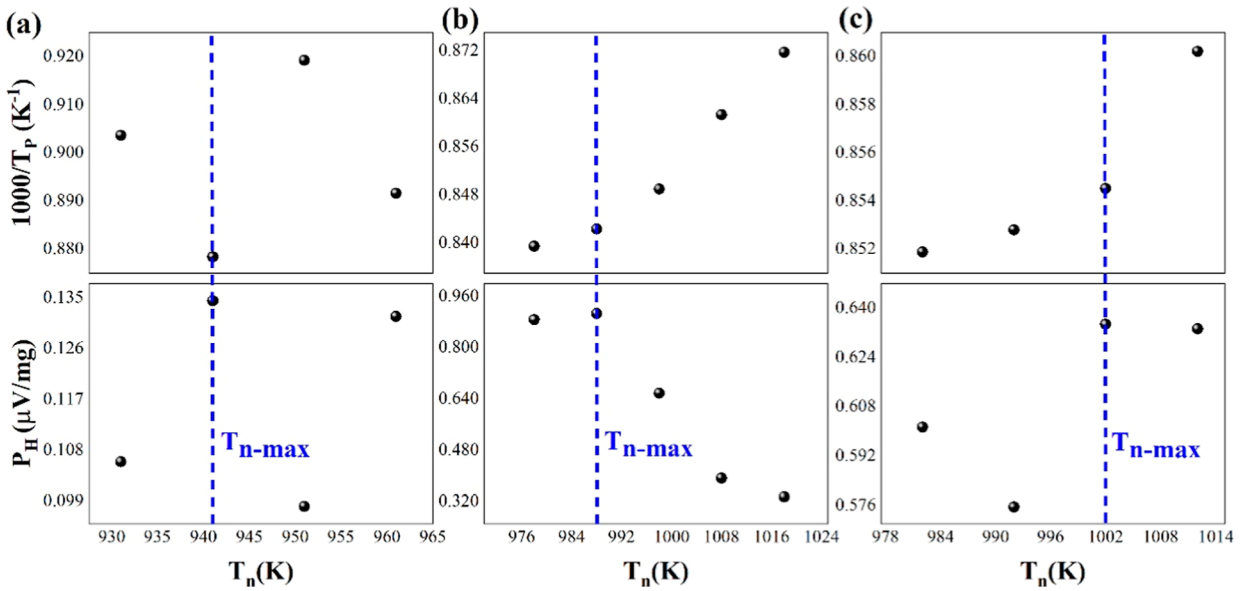

Figure 2. Inverse temperature of the first crystallization peak T_P (top of the figures) and peak height P_H (bottom of the figures) as a function of the temperatures used for nucleation in samples of the compositions: (a) ZAS A; (b) ZAS B; (c) ZAS C. Error bars have been excluded, as the calculated error is negligible compared to the data points.

shows the results of the qualitative analysis of $T_{n\text{-}max}$ for the three ZAS glasses. For compositions ZAS A and ZAS B, T_g (668 and 715 °C, respectively) was selected as the T_n, whereas for composition ZAS C, T_g + 10 °C = 729 °C was considered as the optimum value for T_n.

The crystallization kinetics was evaluated through the nonisothermal Kissinger method. The Kissinger plots and the calculated E_a values are presented in Figure 3.

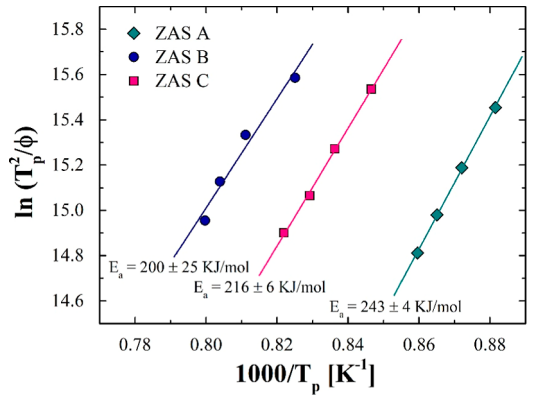

Figure 3. Kissinger plot for the ZAS glasses. The solid straight lines correspond to the linear fit of the experimental data. Error bars have been excluded, as the calculated error is negligible compared to the data points.

Considering the error, the activation energies for ZAS B and ZAS C glasses are very similar, whereas the E_a of ZAS A is slightly higher than those of the other two glasses.

3.2. X-ray Diffraction Analysis. Figure 4 shows the X-ray diffraction (XRD) patterns of the glasses and their corresponding GCs. The heat treatments and the sample names are detailed in Table 2.

To infer the effect of the ZrO_2/TiO_2 ratio on the development of the different crystalline phases, a comparison between the diffraction patterns of GCs from ZAS A, ZAS B, and ZAS C obtained through the same heat treatment protocol and the same XRD conditions (3 h at T_n and 2 h at T_p) is presented in Figure 5.

Figure 5 shows that the crystallization peaks detected in ZAS A (the composition containing TiO_2 as the only nucleating agent) are slightly less sharp than those found in the ZAS B and ZAS C diffractograms. The crystallite sizes of gahnite estimated via the Scherrer equation (eq 2) for each GC prepared are plotted in Figure 6.

Figure 6 shows that, even when the error bars are considered, there is still an important crystallite size difference between the GCs from ZAS A compared with those from ZAS B and ZAS C.

3.3. Transmittance and Color. Figure 7 compares the light transmittance of the parent glasses and their corresponding GCs as a function of the wavelength (left) and the colorimetric coordinates L*, a*, and b* determined in the CIE 1931 color space system in a 2D graph (right). For a direct comparison, the colorimetric coordinates are listed in Table S1 and graphically represented in 3D graphs in Figure S1 (Supporting Information).

Figure 8a–c presents the results of the EPR measurements conducted on glasses ZAS A, B, and C, and GCs A6, B6, and C6 at 77 and 295 K (room temperature, RT). From the EPR spectra, no peak corresponding to Ti^{3+}, which could be associated with the samples' color, was detected. However, a signal corresponding to Fe^{3+} ions was found in all glass samples, with an increasing intensity as the TiO_2 content decreased. This behavior is clearer for the spectra obtained at 77 K. On the other hand, the intensity of the Fe^{3+} peak decreases in A6, compared to glass A, and the same peak is not discernible in GCs B6 and C6. The decrease in the Fe^{3+} amount is likely due to the reduction to Fe^{2+} (which cannot be detected by EPR) after partial crystallization or with increasing the TiO_2 content.[17]

3.4. Mechanical Properties. A comparison of the H_v values of the GCs and their parent glasses, along with some representative indentation marks, is presented in Figure 9.

https://doi.org/10.1021/acs.cgd.4c01000
Cryst. Growth Des. 2024, 24, 9914−9924

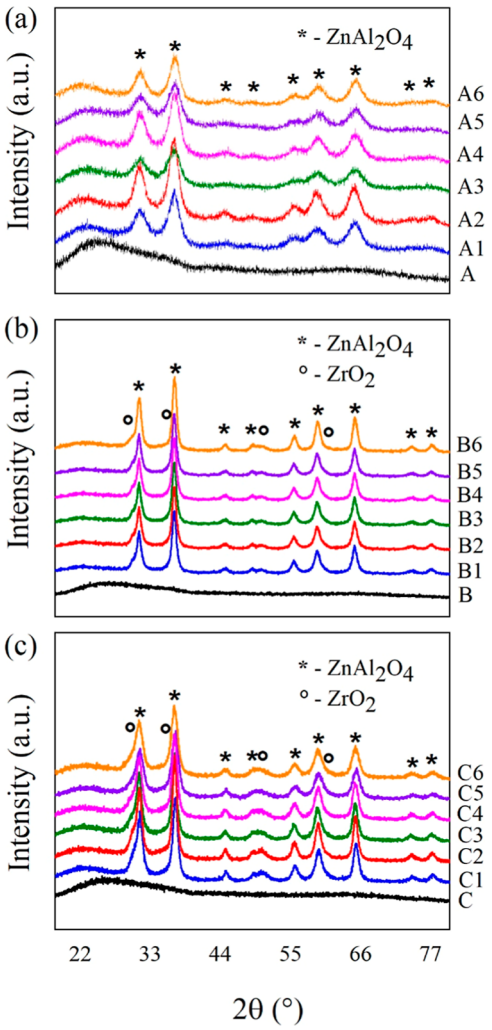

Figure 4. X-ray diffraction patterns of the glasses (A B,C) and GCs (A1-A6, B1−B6, and C1−C6) from (a) ZAS A, (b) ZAS B, and (c) ZAS C. ZrO_2: PDF number 49-1642; $ZnAl_2O_4$: PDF number 74-1138.

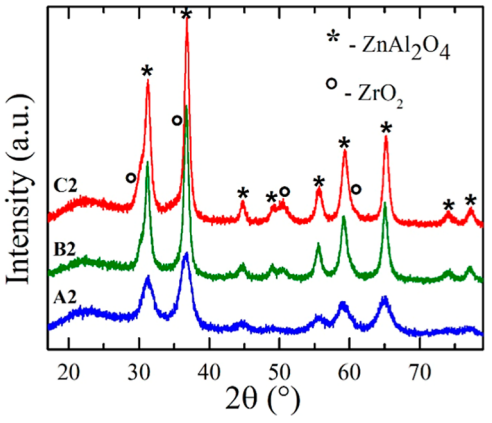

Figure 5. Comparison between the XRD patterns of GCs A2, B2, and C2 obtained through the same heat treatment protocol, corresponding to 3 h at T_n and 2 h at T_p.

4. DISCUSSION

A comparison between the DSC curves (Figure 1) of the different compositions clearly shows that the variation of the ZrO_2/TiO_2 ratio affects the thermal behavior. For instance, the lowest T_g corresponds to the ZAS A glass, which contains TiO_2 as the only nucleating agent, whereas the highest crystallization peak was observed for the ZAS B glass containing both TiO_2 and ZrO_2 as nucleating agents. This difference is related to the distinct effect of TiO_2 and ZrO_2 on the crystallization and the glass structure, despite both having the role of nucleating agents. In aluminosilicate glasses, for instance, TiO_2 acts as a network modifier. In these glasses, an increase in the TiO_2 content decreases both the T_g and the melt viscosity (η) because of the decrease of the network polymerization degree.[33]

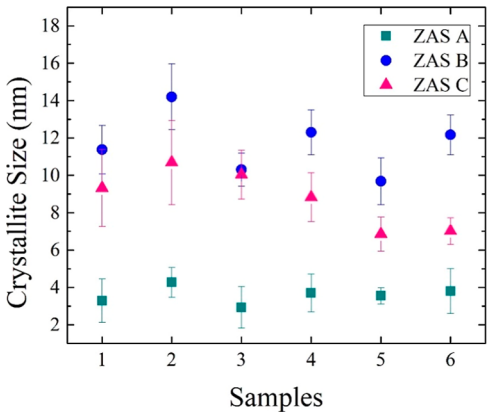

Figure 6. Crystallite sizes of gahnite estimated using eq 2. The numbers 1 to 6 on the horizontal axis designate the heat treatment protocol, as specified in Table 2.

On the other hand, for the same type of glasses, ZrO_2 has an opposite effect on the thermal behavior, providing a higher T_g and a higher η,[34,35] since the Zr^{4+} ions result in a more polymerized silicate network.[36] Despite these different effects, all the precursor glasses analyzed in this study presented a single crystallization peak, indicating that the nucleating agents did not affect the predominant crystalline phase developed, gahnite ($ZnAl_2O_4$). Regardless of the variation in their ZrO_2/TiO_2 ratios, the crystallization of the three glasses was similar, as indicated by the E_a parameter. This outcome is a consequence of the development of the same crystalline phase associated with the single crystallization peak observed in the DSC curves.

The XRD patterns (Figure 4) confirmed that all GCs from ZAS A, B, and C developed $ZnAl_2O_4$ as the main crystalline phase. However, GCs from ZAS B and ZAS C also presented some peaks ascribed to the precipitation of ZrO_2, even though the crystallization of this second phase could not be identified in the DSC curves (Figure 1). Likely, the crystallization peak of ZrO_2 in the DSC curves is not intense enough to be detected or overlaps with the more intense peak, presumably associated with $ZnAl_2O_4$ crystallization. This result of the XRD analysis corroborates those of different studies addressing aluminosilicate glasses containing ZrO_2 as a nucleating agent, which show that ZrO_2 crystals usually precipitate in the early stages of crystallization and behave as nucleation sites for the main crystalline phase.[20,37−39] However, the detection of the crystalline phase ZrO_2 in GCs with both ZrO_2 and TiO_2 intentionally added as nucleating agents contrasts with some works[17,40−42] pointing that $ZrTiO_4$ crystals, developed after an initial liquid−liquid phase separation (LLPS), are responsible for inducing internal nucleation.

https://doi.org/10.1021/acs.cgd.4c01000
Cryst. Growth Des. 2024, 24, 9914−9924

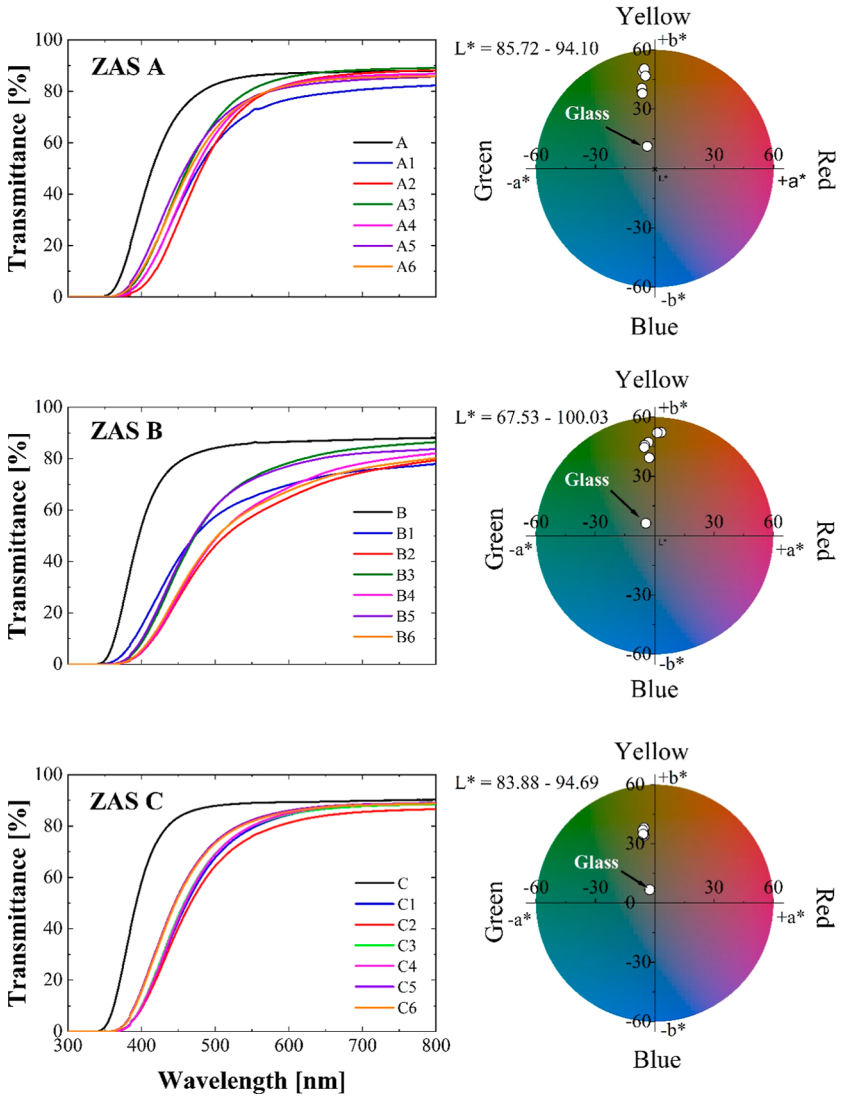

Figure 7. Transmittance as a function of light wavelength (left) and 2D representation of the colorimetric coordinates L*, a*, and b* determined in the CIE 1931 color space system (right) for the parent glasses and their corresponding GCs from compositions (a) ZAS A, (b) ZAS B, and (c) ZAS C. Only the coordinates a* and b* are plotted in the colorimetric maps, which correspond to a transversal section of a color sphere. The range of the longitudinal coordinate L* of each group of samples is indicated at the top left corner of the corresponding map. Samples are approximately 1.5 mm thick.

It is important to note that comparing the XRD peaks for GCs obtained through the same heat treatment protocol (considering the characteristic temperatures of each glass), those associated with the composition ZAS A are less intense (Figure 5). On the other hand, the narrower XRD peaks in GCs from compositions ZAS B and ZAS C can be a consequence of a higher crystal growth rate and/or smaller crystal number density associated with a lower nucleation rate in these compositions with both TiO_2 and ZrO_2.

The XRD patterns of all GCs reveal broad peaks, which are characteristic of nanosized crystallites[43] as confirmed via the Scherrer equation (Figure 6). The composition ZAS A, having TiO_2 as the only nucleating agent, presents the smallest crystallite size. On the other hand, Figure 6 shows that GCs from ZAS B present crystallites larger than those of GCs from ZAS A and C (especially B6), despite being prepared through the same heat treatment protocol. Such behavior is likely due to the higher temperatures selected for the heat treatments of ZAS B since this glass presented the highest T_x and T_p (Table 3). In any case, all values in Figure 6 are smaller than ∼16 nm, explaining the transparency of all GCs. Although the estimation of the crystallite size through the Scherrer equation should ideally be combined with transmission electron microscopy analysis for greater accuracy,[43] eq 2 can be used for average sizes below 100 nm, since in this case, the XRD peak broadening is mostly caused by the crystallite size.[44]

The transmittance spectra (Figure 7) confirm that all GCs have light transmittance percentages relatively similar to those of their corresponding parent glasses, even those heat-treated at higher temperatures, where faster crystal growth is expected. However, crystal size in these GCs is likely conditioned to the high nucleation rates of the parent glass, as a nucleation time of only 3 h is enough to obtain transparent samples. In this case, it is plausible that crystals' impingement and a possible diffusion barrier with a different chemical composition of $ZnAl_2O_4$ around each crystal hinder further crystal growth, limiting them to the nanoscale. The nucleation preceded by LLPS can be another source for the presence of nanosized

https://doi.org/10.1021/acs.cgd.4c01000
Cryst. Growth Des. 2024, 24, 9914−9924

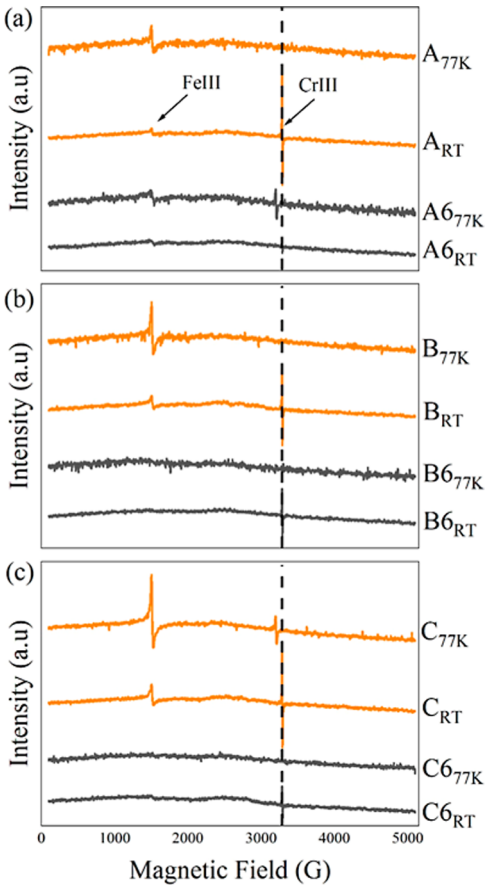

Figure 8. EPR spectra of the parent glasses (a) ZAS A, (b) ZAS B, and (c) ZAS C and some GCs (A6, B6, and C6) at 77 and 295 K (room temperature, RT). Cr^{III} is a standard of g values to calibrate the magnetic field (g = 1.9797). The spectra were normalized by the weight (mg) of each sample. The Fe^{III} signals are described as Fe^{3+} at rhombic symmetry.

crystals, as observed by Golubkov et al.[45] in glasses from the ZAS system containing TiO_2, in which gahnite crystals are formed within the zinc aluminate liquid phase-separated regions of around 6−10 nm. Another possibility for the restriction of the crystals' size to the nanometric scale is the low crystal growth velocity.

Even though all obtained ZAS GCs are transparent to visible light, as can be confirmed in Figure S2 of the Supporting Information, all of them presented a yellowish coloration, as already reported by other studies for glasses nucleated with TiO_2.[14,17,18] In this regard, two charge transfer mechanisms can be proposed: (i) oxygen-to-metal charge transfer (OMCT) transitions (e.g., Ti^{4+}−O^{2}), and (ii) homo (e.g., Ti^{4+}−Ti^{3+}) or heteronuclear (e.g., Fe^{2+}−Ti^{4+}) intervalence charge transfer (IVCT) transitions, as already discussed in other publications for silicate glasses containing TiO_2.[14,17,46]

Both electronic transitions, OMCT and IVCT, are expected to occur in the glasses and GCs of our study due to the presence of Ti ions, which may exist as Ti,[3] Ti^{4+}, or both, and because Fe ions are a common impurity in the raw materials used for the parent glass synthesis.[14,17] Regarding the last aspect, two features associated with Fe^{3+} ions can be identified from the EPR patterns of Figure 8. First, the relative amount of Fe^{3+} increases as the content of TiO_2 decreases, and second, Fe^{3+} is barely identified in the analyzed GGs (Fe^{3+} ions were detected only in the GC A6). Therefore, these results indicate that there is a possible correlation between the decreasing content of TiO_2 and the oxidation state of the proposed coloring ions, likely due to a change of the redox equilibrium $Ti^{3+} + Fe^{3+} \leftrightarrow Ti^{4+} + Fe^{2+}$ from the left to the right side.[17] However, since the EPR measurements did not detect Ti^{3+} ions, we presume that the main cause of the samples' yellowish/brownish coloration and its stronger intensity with the TiO_2 content is likely due to the Ti^{4+}−O^{2-} charge transfer mentioned before.

It is worth mentioning that CeO_2 was added to all the studied compositions aiming to mitigate the original strong yellow-brown color in glasses containing TiO_2, by favoring a Ce (IV) − O(-II) charge transfer. Thus, CeO_2 is reduced, becoming Ce_2O_3 ($4CeO_2 \rightarrow 2Ce_2O_3 + O_2$), and the residual oxygen can oxidize Ti^{3+} to Ti^{4+}.[14] However, the CeO_2 added was not enough to eliminate the yellowish color, and the presence of Ce^{3+} was not identified by EPR.

The colorimetric coordinates L*, a*, and b* (Figure 7), used to quantify the effect of TiO_2 on the color of the studied glasses and GCs, showed that both the chemical composition of the parent glass and the heat treatment affect the color. Overall, the GCs from ZAS C seem to show less scattered results, being concentrated in a relatively small range of values for the a* and b* coordinates. However, considering only the L* coordinate, the GCs from ZAS A compositions showed a smaller variation. GCs from ZAS B presented the highest variation in all coordinates, with samples in two quadrants of the CIELab color space. For the three compositions, the b* (tendency to a yellow-brown coloration) values for the GCs are higher than those of their corresponding parent glass, an outcome mainly attributed to changes in the oxidation state of some ions during heat treatment. Considering only the GCs, those from ZAS C presented the smallest b*, confirming that the decrease of the TiO_2 content, while maintaining the same base glass composition, mitigates the yellowish hue of the samples. It is interesting to note that the b* values for the GCs heat-treated at T_x from ZAS A and from ZAS C are similar, while those obtained from heat treatments at T_p show higher b* values (stronger yellow tone). This behavior can be correlated to the decrease in the Fe^{3+} amount and their possible reduction to Fe^{2+} during crystallization, as shown by the EPR spectra (Figure 8), along with an increasing light scattering caused by larger crystals and/or higher crystallized fraction (Figure S2).

Because of the small effect of the ZrO_2/TiO_2 ratio change on the crystallization kinetics indicated by E_a (Figure 3) and the similar crystal size (nanometric) of the GCs (Figure 6), the H_v of all samples remains in a narrow range of ∼7.0−7.5 GPa (Figure 9). The improvement of the mechanical properties of GCs compared with those of their parent glasses is mostly ascribed to the crystalline phase developed. This can be understood since the hardness of the GCs is a combination of the H_v of both the glassy matrix and the crystal phase (gahnite, $ZnAl_2O_4$), which has a H_v around 10.5−12.6 GPa in fully polycrystalline samples.[47,48] The presence of nanocrystals and the same predominant crystal phase in all the studied GCs indicates that the variation in the chemical composition of the parent glass was not enough to affect H_v. Therefore, the partial replacement of TiO_2 with ZrO_2 enables the preparation of glasses and GCs with a lighter yellow color, without impairing their mechanical performance, i.e., by controlling the nucleating agents ZrO_2/TiO_2 ratio of a selected ZAS base

https://doi.org/10.1021/acs.cgd.4c01000
Cryst. Growth Des. 2024, 24, 9914−9924

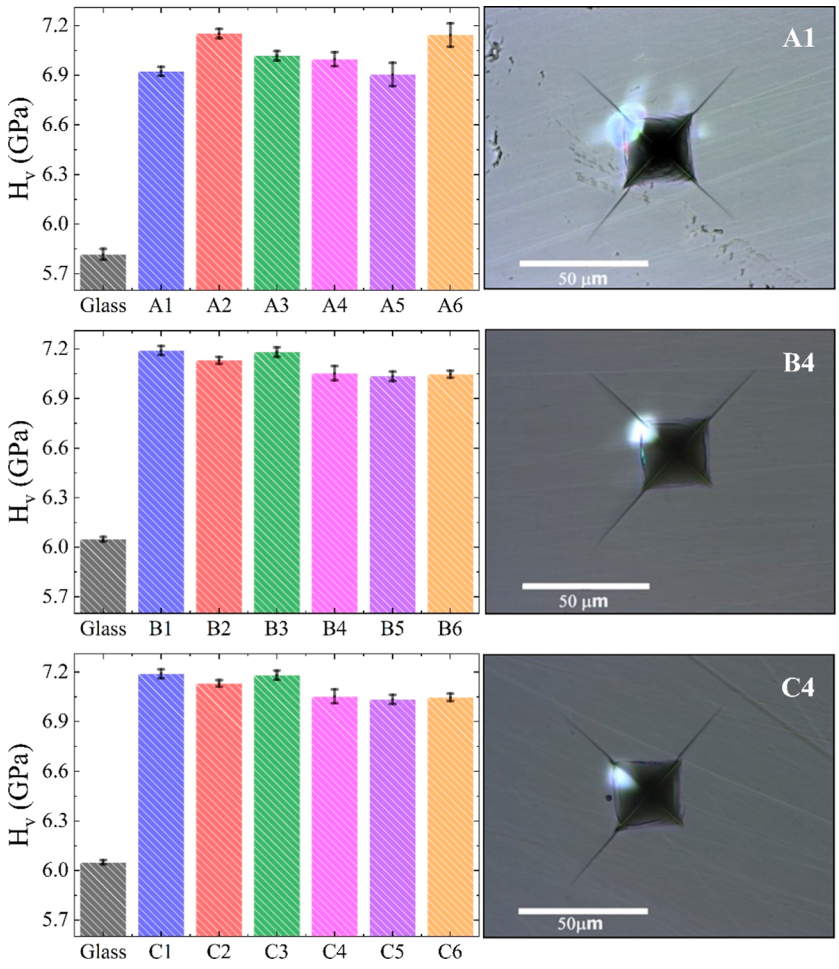

Figure 9. Vickers microhardness of the glasses and GCs from (a) ZAS A, (b) ZAS B, and (c) ZAS C. Representative indentations from one GC of each composition are presented on the right-hand side.

glass composition it was possible to increase the transparency of the obtained glasses and GCs while keeping the hardness unchanged.

Finally, for the sake of comparison, we prepared another glass with the same base glass composition, i.e., the same proportion between the oxides (except the nucleating agents) of the ZAS A, ZAS B, and ZAS C glasses, but containing 3 mol % of ZrO_2 (as for ZAS C) as the only nucleating agent (named as ZAS Z). According to the results presented in the Appendix, the characteristic temperatures for this glass are higher than those of ZAS A, ZAS B, and ZAS C, and a longer nucleation treatment (at least for 72 h) is necessary to yield transparent GCs. Additionally, the H_v for GCs from ZAS Z is close to values measured for GCs from ZAS A, ZAS B, and ZAS C.

Additional experimental data (viz, colorimetric coordinates L*, a*, and b* in the CIE 1931 color space, their three-dimensional representation, and images of all samples to show their external appearance) are available in the Supporting Information to complement the discussion of this work.

5. CONCLUSIONS

This study investigated the impact of varying the ZrO_2/TiO_2 nucleating agent ratio on the crystallization behavior, color, transparency, and hardness of ZAS-based glasses and glass-ceramics (GCs). Considering the visual appearance of the glasses and GCs, CIELab analysis confirmed that the partial replacement of TiO_2 with ZrO_2 mitigates the unwanted yellow/brown coloration, presumably caused by the presence of $Ti^{4+}-O^{2-}$ charge transfer bands and different charge transfer mechanisms between Ti and Fe ions, these latter detected via EPR. Additionally, Since the changes in the ZrO_2/TiO_2 ratio had a minimal effect on the crystallization kinetics, the hardness of the evaluated glasses and GCs was similar. The best balance between mechanical and optical properties was achieved for the samples from the ZAS C composition, with a ZrO_2/TiO_2 = 2:1 ratio. These outcomes offer valuable insights for tailoring the hardness and optical properties of ZAS GCs through the controlled substitution of TiO_2 with ZrO_2, providing guidance for developing esthetically pleasing, high-performance materials.

APPENDIX ZNO–AL_2O_3–SIO_2 COMPOSITION WITH ZRO_2 AS THE ONLY NUCLEATING AGENT (ZAS Z)

The nominal composition of the glass ZAS Z in mol % corresponds to 16.5 ZnO·16.5 Al_2O_3·61.6 SiO_2·2.3 K_2O·3.0 ZrO_2. This is the same base composition of glasses ZAS A, ZAS B, and ZAS C, but with a lower nucleating agent's content compared with ZAS B and ZAS C, and a similar content in wt % of nucleating agent compared to ZAS A. This adjustment in the nucleating agent content was necessary to avoid having a

https://doi.org/10.1021/acs.cgd.4c01000
Cryst. Growth Des. 2024, 24, 9914−9924

considerable amount of ZrO_2 (≥4.5 mol %), which would make homogenization during melting difficult.

From the DSC curve (Figure S3, Supporting Information), two crystallization peaks can be observed: the first, around 996 °C, probably related to the precipitation of zirconia, and the second, at 1064 °C, assigned to the crystallization of gahnite. The T_g (734 °C) and the T_{P2} of the glass ZAS Z exhibited an increase compared to the same parameters of the other ZAS compositions investigated in this study (Table 3).

The heat treatments for the glass ZAS Z were defined based on its characteristic temperatures (Table S2, Supporting Information). Because of the absence of TiO_2, the as-quenched ZAS Z glass is colorless, as shown in Table S2. In contrast to the glasses ZAS A, ZAS B, and ZAS C, the transparency of the GCs from ZAS Z is highly dependent on the nucleation time. The samples nucleated at 734 °C for 3 h and subjected to crystal growth at 974 and 996 °C (onset and maximum temperature of the first crystallization peak, respectively) for 2 h are completely opaque (Table S2, second and third rows). Increasing the nucleation time from 3 to 24 h at 734 °C, followed by crystal growth at the onset of the first crystallization peak (~974 °C), seems to reduce the opacity of the resulting GC (Table S2, fourth row).

Further nucleation treatments at T_g for 48, 72, 96, and 120 h, followed by crystal growth at the onset of the first crystallization peak for 2 h, increase the translucency of all samples, as shown in the fifth to eighth rows of Table S2. However, even the translucent and transparent samples exhibit a yellowish tone, which can be attributed to the birefringence of the ZrO_2 tetragonal structure, becoming more evident when compared to the parent glass (first row in Table S2). A similar visual trend was observed in GCs subjected to crystal growth around the second crystallization peak (~1064 °C); as the nucleation time increased, opacity decreased. The heat treatment, visual aspect, and H_v of the glass and some selected GCs from composition ZAS Z are summarized in Table S2. All samples in Table S2 have similar thicknesses (~3 mm).

XRD measurements were conducted on bulk and polished GCs to identify the crystalline phases. Similar to compositions ZAS B and C, only two crystalline phases were identified: zirconia and gahnite (Figure S4, Supporting Information).

Table S2 also shows the results for the H_v measurements, which were conducted on GCs obtained through different heat-treatment protocols. The samples were tested using a Vickers indenter and loads of 10 and 20N with a dwell time of 15 s. The samples nucleated for only 3 h consistently developed cracks at the corner of the impressions when a load of 20 N was applied. All the other samples were tested with a load of 10 N. The results for all GCs range from 6.8 to 7.7 GPa, similar to the values measured for ZAS A, ZAS B, and ZAS C GCs. In general, samples nucleated for longer times showed higher hardness (Table S2), and the same trend was observed for samples heat-treated at both the first and second crystallization peaks.

The average crystallite diameter of the GCs from ZAS Z (Table S3) was estimated using Scherrer equation eq 2, and the same correction regarding the instrumental broadening contribution applied for compositions ZAS A, B, and C (Section 2.3) was considered in this case. As expected, the transparency of the samples increases as the crystallite size decreases (Table S3) because of the longer nucleation time. The opaque samples (three first rows of Table S2) have an average crystallite size of 32 nm, whereas the samples showing a higher degree of translucency/transparency (last two rows of Table S3) have an average crystallite size of 17 nm, a value close to those estimated for the transparent samples of compositions ZAS A, ZAS B, and ZAS C (Figure 6).

In summary, these results indicate that the total replacement of TiO_2 by ZrO_2, using a content of 3 mol % of ZrO_2 instead of 4.5 mol %, does not enhance either the transmittance or the mechanical performance of transparent ZAS GCs. Additionally, increasing the ZrO_2 content (>4.5 mol %) may be detrimental to the melting and homogenization processes of the parent glass.

■ ASSOCIATED CONTENT

Supporting Information

The Supporting Information is available free of charge at https://pubs.acs.org/doi/10.1021/acs.cgd.4c01000.

Table S1. Colorimetric coordinates L*, a*, and b* in the CIE 1931 color space of ZAS glasses and GCs. Figure S.1. Tridimensional representation of the colorimetric coordinates L*, a*, and b* determined in the CIE 1931 color space for the parent glass and the corresponding GCs of compositions: (a) ZAS A, (b) ZAS B, and (c) ZAS C. Figure S.2. (a) Transparent visual aspect of the glasses and GCs from ZAS A, B, and C. (b) The paper sheet is approximately 6 cm far from the samples. Figure S.3. DSC curve of the glass ZAS Z. Table S2. Heat treatments, external appearance, and H_v of selected samples from composition ZAS Z. Figure S.4. X-ray diffraction pattern of the sample nucleated at T_g for 3 h and crystallized at 996 °C for 2 h (first crystallization peak according to Figure S.3). Table S3. Crystallite size estimates according to Scherrer equation (PDF)

■ AUTHOR INFORMATION

Corresponding Author

Lorena Raphael Rodrigues − *Department of Materials Engineering, Center for Research, Technology, and Education in Vitreous Materials, Federal University of São Carlos, São Paulo 13565-905, Brazil; Department of Metallurgy, Federal Institute of Espírito Santo, Vitória, Espírito Santo 29040-780, Brazil;* orcid.org/0000-0002-7270-6040; Email: lorena.raphael92@gmail.com

Authors

Gisele Guimarães dos Santos − *Department of Materials Engineering, Center for Research, Technology, and Education in Vitreous Materials, Federal University of São Carlos, São Paulo 13565-905, Brazil; Department of Materials Science and Engineering, University of Wisconsin−Madison, 1509 University Avenue, Madison, Wisconsin 53706, United States;* orcid.org/0000-0001-7136-5494

María Helena Ramírez Acosta − *Department of Materials Engineering, Center for Research, Technology, and Education in Vitreous Materials, Federal University of São Carlos, São Paulo 13565-905, Brazil*

Akio Koike − *Materials Integration Laboratories, AGC Inc, Yokohama, Kanagawa 230-0045, Japan*

Shusaku Akiba − *Materials Integration Laboratories, AGC Inc, Yokohama, Kanagawa 230-0045, Japan*

Shigeki Sawamura − *Materials Integration Laboratories, AGC Inc, Yokohama, Kanagawa 230-0045, Japan*

https://doi.org/10.1021/acs.cgd.4c01000
Cryst. Growth Des. 2024, 24, 9914−9924

Satoshi Yoshida − *Materials Integration Laboratories, AGC Inc, Yokohama, Kanagawa 230-0045, Japan*
Valmor Roberto Mastelaro − *São Carlos Institute of Physics, University of São Paulo, São Paulo 13566-590, Brazil;* orcid.org/0000-0001-9512-4214
Otaciro Rangel Nascimento − *São Carlos Institute of Physics, University of São Paulo, São Paulo 13566-590, Brazil*
Edgar Dutra Zanotto − *Department of Materials Engineering, Center for Research, Technology, and Education in Vitreous Materials, Federal University of São Carlos, São Paulo 13565-905, Brazil;* orcid.org/0000-0003-4931-4505

Complete contact information is available at: https://pubs.acs.org/10.1021/acs.cgd.4c01000

Funding

The Article Processing Charge for the publication of this research was funded by the Coordination for the Improvement of Higher Education Personnel - CAPES (ROR identifier: 00x0ma614).

Notes

The authors declare no competing financial interest.

■ ACKNOWLEDGMENTS

This work was partially supported by the São Paulo Research Foundation (FAPESP) through the CEPID project no. 2013/07793-6 and by the National Council for Scientific and Technological Development (CNPq).

■ REFERENCES

(1) Deubener, J.; Allix, M.; Davis, M. J.; Duran, A.; Höche, T.; Honma, T.; Komatsu, T.; Krüger, S.; Mitra, I.; Müller, R.; Nakane, S.; Pascual, M. J.; Schmelzer, J. W. P.; Zanotto, E. D.; Zhou, S. Updated Definition of Glass-Ceramics. *J. Non-Cryst. Solids* **2018**, *501*, 3−10.
(2) Fernandes, H. R.; Gaddam, A.; Rebelo, A.; Brazete, D.; Stan, G. E.; Ferreira, J. M. F. Bioactive Glasses and Glass-Ceramics for Healthcare Applications in Bone Regeneration and Tissue Engineering. *Mater.* **2018**, *11*, 2530.
(3) Montazerian, M.; Baino, F.; Fiume, E.; Migneco, C.; Alaghmandfard, A.; Sedighi, O.; DeCeanne, A. V.; Wilkinson, C. J.; Mauro, J. C. Glass-Ceramics in Dentistry: Fundamentals, Technologies, Experimental Techniques, Applications, and Open Issues. *Prog. Mater. Sci.* **2023**, *132*, 101023.
(4) Gallo, L. S. A.; Villas Boas, M. O. C.; Rodrigues, A. C. M.; Melo, F. C. L.; Zanotto, E. D. Transparent Glass-Ceramics for Ballistic Protection: Materials and Challenges. *J. Mater. Res. Technol.* **2019**, *8*, 3357−3372.
(5) de Araújo, C. B.; Kassab, L. R. P.; da Silva, D. M. Optical Properties of Glasses and Glass-Ceramics for Optical Amplifiers, Photovoltaic Devices, Color Displays, Optical Limiters, and Random Lasers. *Opt. Mater.* **2022**, *131*, 112648.
(6) Chakrabarti, A.; Menon, S.; Tarafder, A.; Molla, A. R. Glass−Ceramics: A Potential Material for Energy Storage and Photonic Applications. In *In Glasses and Glass-Ceramics*; Springer: Singapore, 2022; .
(7) Shang, F.; Wei, J.; Xu, J.; Zhang, G.; Li, M.; Xu, K.; Liu, X.; Li, B.; Huang, H.; Chen, G.; Xu, H. Glass-Ceramic Capacitors with Simultaneously High Power and Energy Densities under Practical Charge−Discharge Conditions. *ACS Appl. Mater. Interfaces* **2022**, *14* (47), 53081−53089.
(8) Zitani, M. K.; Ebadzadeh, T.; Banijamali, S.; Riahifar, R.; Rüssel, C.; Abkenar, S. K.; Ren, H. High Quality Factor Microwave Dielectric Diopside Glass-Ceramics for the Low Temperature Co-Fired Ceramic (LTCC) Applications. *J. Non-Cryst. Solids* **2018**, *487*, 65−71.
(9) Dymshits, O.; Shepilov, M.; Zhilin, A. Transparent Glass-Ceramics for Optical Applications. *MRS Bull.* **2017**, *42* (03), 200−205.
(10) Kumar, S. A Review on Zerodur Material Strength Behaviour with Lightweighted Design. *Mater. Today: Proc.* **2021**, *37*, 3643−3645.
(11) SCHOTT. Zerodur. https://www.schott.com/en-au/products/zerodur-P1000269/applications (accessed 13 02, 2024).
(12) Senk, M. V.; Mathias, I.; Zanotto, E. D.; Serbena, F. C. Crystallized Fraction and Crystal Size Effects on the Strength and Toughness of Lithium Disilicate Glass-Ceramics. *J. Eur. Ceram. Soc.* **2023**, *43*, 3600−3609.
(13) Beall, G. H.; Duke, D. A. Transparent Glass-Ceramics. *J. Mater. Sci.* **1969**, *4*, 340−352.
(14) Molla, A. R.; Rodrigues, A. M.; Singh, S. P.; Lancelotti, R. F.; Zanotto, E. D.; Rodrigues, A. C. M.; Reza Dousti, M.; de Camargo, A. S. S.; Magon, C. J.; Silva, I. D. A. Crystallization, Mechanical, and Optical Properties of Transparent, Nanocrystalline Gahnite Glass-Ceramics. *J. Am. Ceram. Soc.* **2017**, *100* (5), 1963−1975.
(15) DeCeanne, A. V.; Rodrigues, L. R.; Wilkinson, C. J.; Mauro, J. C.; Zanotto, E. D. Examining the Role of Nucleating Agents within Glass-Ceramic Systems. *J. Non-Cryst. Solids* **2022**, *591* (March), 121714.
(16) Kurajica, S.; Šipušić, J.; Zupancic, M.; Brautović, I.; Albrecht, M. ZnO-Al2O3-SiO2 Glass Ceramics: Influence of Composition on Crystal Phases, Crystallite Size and Appearance. *J. Non-Cryst. Solids* **2021**, *553*, 120481.
(17) Chavoutier, M.; Caurant, D.; Majérus, O.; Boulesteix, R.; Loiseau, P.; Jousseaume, C.; Brunet, E.; Lecomte, E. Effect of TiO2 Content on the Crystallization and the Color of (ZrO_2,TiO_2)-Doped Li_2O-Al_2O_3-SiO_2 Glasses. *J. Non-Cryst. Solids* **2014**, *384*, 15−24.
(18) Wange, P.; Höche, T.; Rüssel, C.; Dieter Schnapp, J. Microstructure-Property Relationship in High-Strength MgO-Al_2O_3-SiO_2-TiO_2 Glass-Ceramics. *J. Non-Cryst. Solids* **2002**, *298* (2−3), 137−145.
(19) El-shafi, N. A.; Morsi, M. M. Optical Absorption and Infrared Studies of Some Silicate Glasses Containing Titanium. *J. Mater. Sci.* **1997**, *32*, 5185−5189.
(20) Kleebusch, E.; Patzig, C.; Höche, T.; Rüssel, C. Phase Formation during Crystallization of a Li_2O-Al_2O_3-SiO_2 Glass with ZrO_2 as Nucleating Agent − An X-Ray Diffraction and (S)TEM-Study. *Ceram. Int.* **2017**, *43*, 9769−9777.
(21) Huang, J.; Zhang, J.; Yu, Y.; Bai, H.; Zhang, Z.; Huang, Y. Transparent MgO-Al_2O_3-SiO_2 Glass-Ceramics Prepared with ZrO_2 and SnO_2 as Nucleating Agents. *J. Non-Cryst. Solids* **2022**, *588*, 121585.
(22) Patzig, C.; Dittmer, M.; Gawronski, A.; Höche, T.; Rüssel, C. Crystallization of ZrO_2-Nucleated MgO/Al_2O_3/SiO_2 Glasses-a TEM Study. *CrystEngComm* **2014**, *16* (29), 6578−6587.
(23) Krüger, S.; Deubener, J.; Ritzberger, C.; Höland, W. Nucleation Kinetics of Lithium Metasilicate in ZrO_2-Bearing Lithium Disilicate Glasses for Dental Application. *Int. J. Appl. Glass Sci.* **2013**, *4* (1), 9−19.
(24) Sun, Q.; Shi, J. Calculation and Prediction the Charge Transfer Energy of O^{2-}-Zr^{4+} in Inorganic Crystals. *J. Phys. Chem. C* **2010**, *114* (7), 3230−3234.
(25) Xia, X.; Dutta, I.; Mauro, J. C.; Aitken, B. G.; Kelton, K. F. Temperature dependence of crystal nucleation in BaO·2SiO2 and 5BaO·8SiO2 glasses using differential thermal analysis. *J. Non-Cryst. Solids* **2017**, *459*, 45−50.
(26) Kissinger, H. E. Reaction Kinetics in Differential Thermal Analysis. *Anal. Chem.* **1957**, *29*, 1702−1706.
(27) Langford, J. I.; Wilson, A. J. C. Seherrer after Sixty Years: A Survey and Some New Results in the Determination of Crystallite Size. *J. Appl. Crystallogr.* **1978**, *11*, 102−113.
(28) Durmus, D. CIELAB color space boundaries under theoretical spectra and 99 test color samples. *Color Res. Appl.* **2020**, *45* (5), 796−802.

(29) Biswas, J.; Jana, S. Comparative Studies on CIELab, Thermal and Optical Characteristics of Dysprosium (Dy3+) Incorporated Phospho-Tellurite Glasses for White Light Generation. *Opt. Mater.* **2023**, *141*, 113932.
(30) Seymour, J. Color Inconstancy in CIELAB: A Red Herring? *Color Res. Appl.* **2022**, *47* (4), 900−919.
(31) ASTM International. *C1327 − 15: Standard Test Method for Vickers Indentation Hardness of Advanced Ceramics*, 2019..
(32) Marotta, A.; Buri, A.; Branda, F.; Saiello, S. *Nucleation and Crystallization of $Li_2O_2SiO_2$ Glass - A DTA Study*; American Ceramic Society, 1982; Vol. *4*.
(33) Wang, Z.; Xu, R. Effects of TiO_2 on the Structural Characteristics of $CaO−SiO_2−Al_2O_3−TiO_2$ Glass in the Same Superheat State Studied by Raman Spectra. *Ceram. Int.* **2023**, *49* (16), 26494−26504.
(34) Thieme, K.; Rüssel, C. Nucleation and Growth Kinetics and Phase Analysis in Zirconia-Containing Lithium Disilicate Glass. *J. Mater. Sci.* **2015**, *50*, 1488−1499.
(35) Zhu, L.; Wang, M.; Xu, Y.; Zhang, X.; Lu, P. Dual Effect of ZrO_2 on Phase Separation and Crystallization in $Li_2O−Al_2O_3−SiO_2−P_2O_5$ Glasses. *J. Am. Ceram. Soc.* **2022**, *105* (9), 5698−5710.
(36) Lin, C. C.; Shen, P.; Chang, H. M.; Yang, Y. J. Composition Dependent Structure and Elasticity of Lithium Silicate Glasses: Effect of ZrO_2 Additive and the Combination of Alkali Silicate Glasses. *J. Eur. Ceram. Soc.* **2006**, *26* (16), 3613−3620.
(37) Patzig, C.; Höche, T.; Dittmer, M.; Rüssel, C. Temporal Evolution of Crystallization in $MgO-Al_2O_3-SiO_2-ZrO_2$ Glass Ceramics. *Cryst. Growth Des.* **2012**, *12* (4), 2059−2067.
(38) Dressler, M.; Rüdinger, B.; Deubener, J. Crystallization Kinetics in a Lithium Alumosilicate Glass Using SnO_2 and ZrO_2 Additives. *J. Non-Cryst. Solids* **2014**, *389*, 60−65.
(39) Patzig, C.; Höche, T.; Hu, Y.; Ikeno, H.; Krause, M.; Dittmer, M.; Gawronski, A.; Rüssel, C.; Tanaka, I.; Henderson, G. S. Zr Coordination Change during Crystallization of $MgO-Al_2O_3-SiO_2-ZrO_2$ Glass Ceramics. *J. Non-Cryst. Solids* **2014**, *384*, 47−54.
(40) He, D.; Ma, H.; Zhong, H. Effect of Different Nucleating Agent Ratios on the Crystallization and Properties of MAS Glass Ceramics. *J. Eur. Ceram. Soc.* **2021**, *41* (16), 342−350.
(41) Höche, T.; Patzig, C.; Gemming, T.; Wurth, R.; Rüssel, C.; Avramov, I. Temporal Evolution of Diffusion Barriers Surrounding $ZrTiO_4$ Nuclei in Lithia Aluminosilicate Glass-Ceramics. *Cryst. Growth Des.* **2012**, *12* (3), 1556−1563.
(42) Bhattacharyya, S.; Höche, T.; Jinschek, J. R.; Avramov, I.; Wurth, R.; Müller, M.; Rüssel, C. Direct Evidence of Al-Rich Layers around Nanosized $ZrTiO_4$ in Glass: Putting the Role of Nucleation Agents in Perspective. *Cryst. Growth Des.* **2010**, *10* (1), 379−385.
(43) Hassanzadeh-Tabrizi, S. A. Precise Calculation of Crystallite Size of Nanomaterials: A Review. *J. Alloys Compd.* **2023**, *968*, 171914.
(44) Holzwarth, U.; Gibson, N. The Scherrer Equation versus the "Debye-Scherrer Equation. *Nat. Nanotechnol.* **2011**, *6*, 534.
(45) Golubkov, V. V.; Dymshits, O. S.; Petrov, V. I.; Shashkin, A. V.; Tsenter, M. Y.; Zhilin, A. A.; Kang, U. Small-Angle X-Ray Scattering and Low-Frequency Raman Scattering Study of Liquid Phase Separation and Crystallization in Titania-Containing Glasses of the $ZnO-Al_2O_3-SiO_2$ System. *J. Non-Cryst. Solids* **2005**, *351* (8−9), 711−721.
(46) Eremeev, K.; Dymshits, O.; Alekseeva, I.; Khubetsov, A.; Zapalova, S.; Tsenter, M.; Basyrova, L.; Serres, J. M.; Mateos, X.; Loiko, P.; Popkov, V.; Zhilin, A. Effect of Redox Conditions of Glass Melting on the Structure and the Properties of Titanium-Containing Gahnite Glass-Ceramics. *J. Eur. Ceram. Soc.* **2024**, *44* (5), 3362−3380.
(47) Sokol, M.; Meir, S.; Strumza, E.; Kalabukhov, S.; Hayun, S.; Frage, N. On the Effects of LiF on the Synthesis and Reactive Sintering of Gahnite ($ZnAl_2O_4$). *Ceram. Int.* **2017**, *43* (17), 14891−14896.
(48) Goldstein, A.; Yeshurun, Y.; Vulfson, M.; Kravits, H. Fabrication of Transparent Polycrystalline <scp>ZnAl</scp>$_2$<scp>O</scp>$_4$ − A New Optical Bulk Ceramic. *J. Am. Ceram. Soc.* **2012**, *95* (3), 879−882.

https://doi.org/10.1021/acs.cgd.4c01000
Cryst. Growth Des. 2024, 24, 9914−9924